Supporting information

Realizing High Thermoelectric Performance in Non-nanostructured n-type PbTe

Baohai Jia, [ab] Yi Huang, [a] Yan Wang, [a] Yeshiyuan Zhou, [a] Xiaodie Zhao, [c] Suiting Ning, [c] Xiao Xu, [a] Peijian Lin, [a] Zhiquan Chen,[c] Binbin Jiang, *[a] Jiaqing He, *[ab]

[a]Shenzhen Key Laboratory of Thermoelectric Materials, Department of Physics, Southern University of Science and Technology, Shenzhen 518055, China.

[b]Guangdong-Hong Kong-Macao Joint Laboratory for Photonic-Thermal-Electrical Energy Materials and Devices, Southern University of Science and Technology, Shenzhen 518055, China.

[c]Hubei Nuclear Solid Physics Key Laboratory, Department of Physics, Wuhan University, Wuhan 430072, China.

1. Calculation of room-temperature Hall carrier mobility as a function of the carrier concentration

The Hall mobility can be expressed as:

$$\mu_{\mathrm{H}} = \frac{e\tau_0 F_{-\frac{1}{2}}(\eta)}{2m^* F_0(\eta)}, \tag{1}$$

where e is a quantity of unity charge, m* is the effective $\hbar$ mass of the charge carriers. $F_n(\eta)$ is Fermi integral calculated from specific reduced chemical potential, $\eta = E_F/kT$. τ_0 is the relaxation time, which is related to the energy in the case of acoustic phonon scattering, and can be defined as

$$\tau_0 = \frac{\pi\hbar^4 C_{11}}{\sqrt{2}E_{\mathrm{def}}^2(m^* kT)^{3/2}}, \tag{2}$$

in n-type PbTe, C_{11}=105.3 GPa and E_{def}=24 eV, the former is a combination of elastic constant and the latter denotes the deformation potential and describes the carrier scattering strength by acoustic phonons.

The parameter η is a specific reduced chemical potential, which can be deduced from the Hall charge-carrier concentration

$$n_{\mathrm{H}} = 4\pi\left(\frac{2\mathrm{m}^* \mathrm{kT}}{h^2}\right)^{3/2}\frac{F_{-\frac{1}{2}}(\eta)}{r_{\mathrm{H}}}, \tag{3}$$

where r_H is the Hall factor and defined as

$$r_{\mathrm{H}} = \frac{3}{2}F_{\frac{1}{2}}(\eta)\frac{F_{-\frac{1}{2}}(\eta)}{2F_0^2(\eta)}. \tag{4}$$

2. The XRD, thermoelectric properties, and hall measurements of iodine doping PbTe

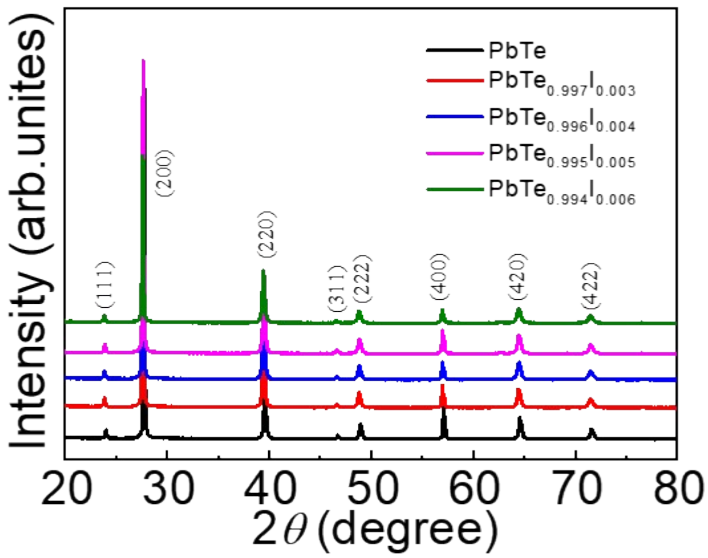

Figure S1. XRD patterns for samples of $PbTe_{1-x}I_x$ (x =0 ~ 0.006).

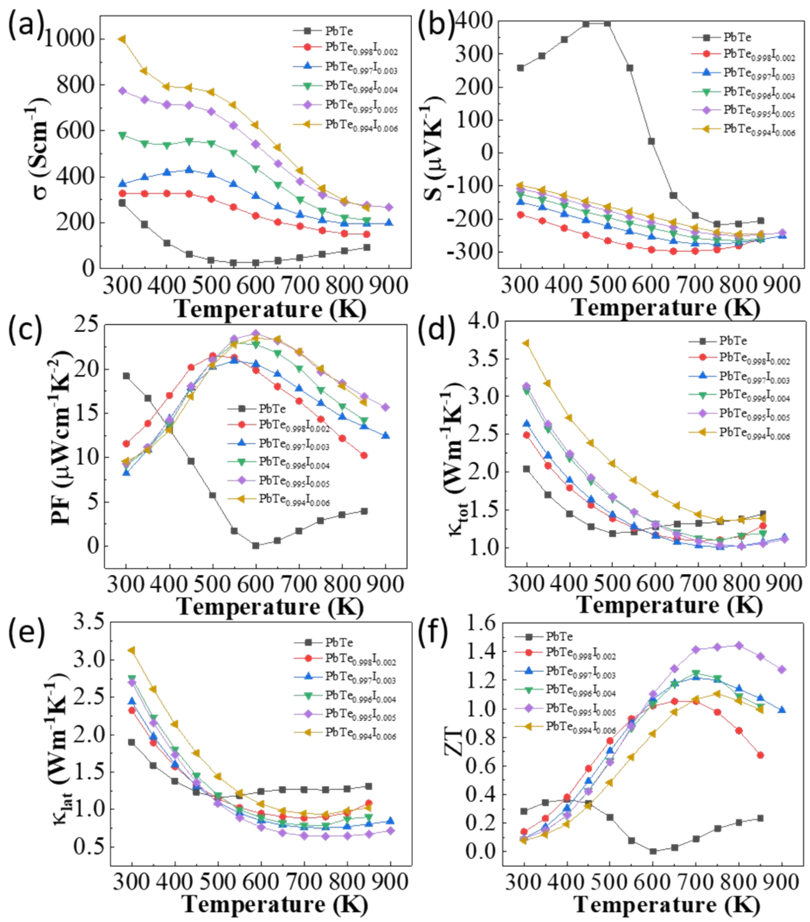

Figure S2. Temperature-dependent thermoelectric properties of $PbTe_{1-x}I_x$ (x =0 ~ 0.006), (a) electrical conductivity, (b) Seeebeck coefficient, (c) power factor, (d) total thermal conductivity, (e) lattice thermal conductivity, (f) *zT* value.

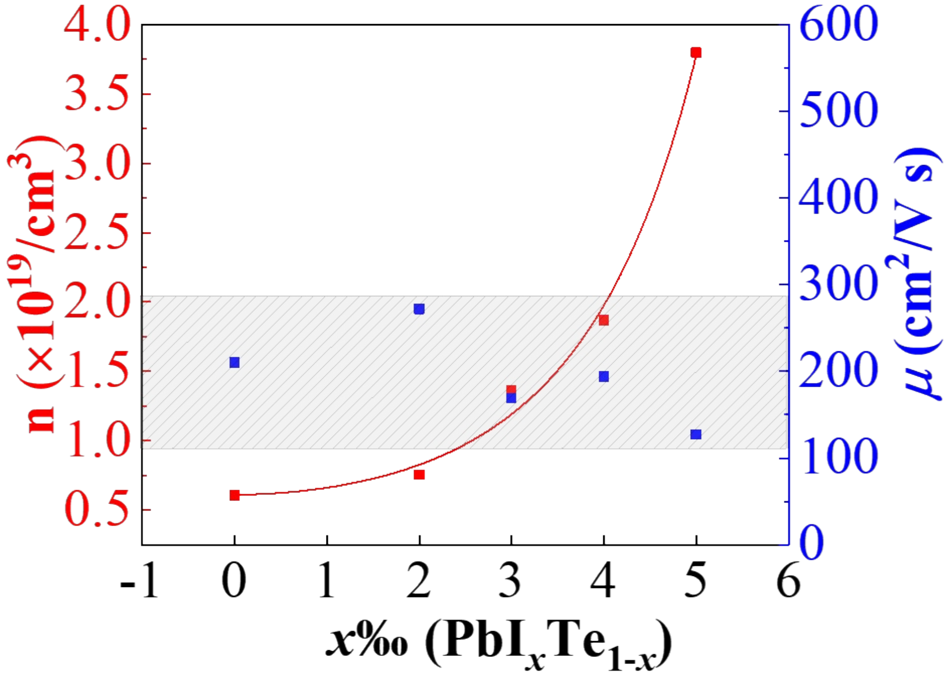

Figure S3. Hall measurements of $PbTe_{1-x}I_x$ (x =0 ~ 0.005).

3. The XRD and electrical transport of $PbTe_{0.997-y}S_yI_{0.003}$

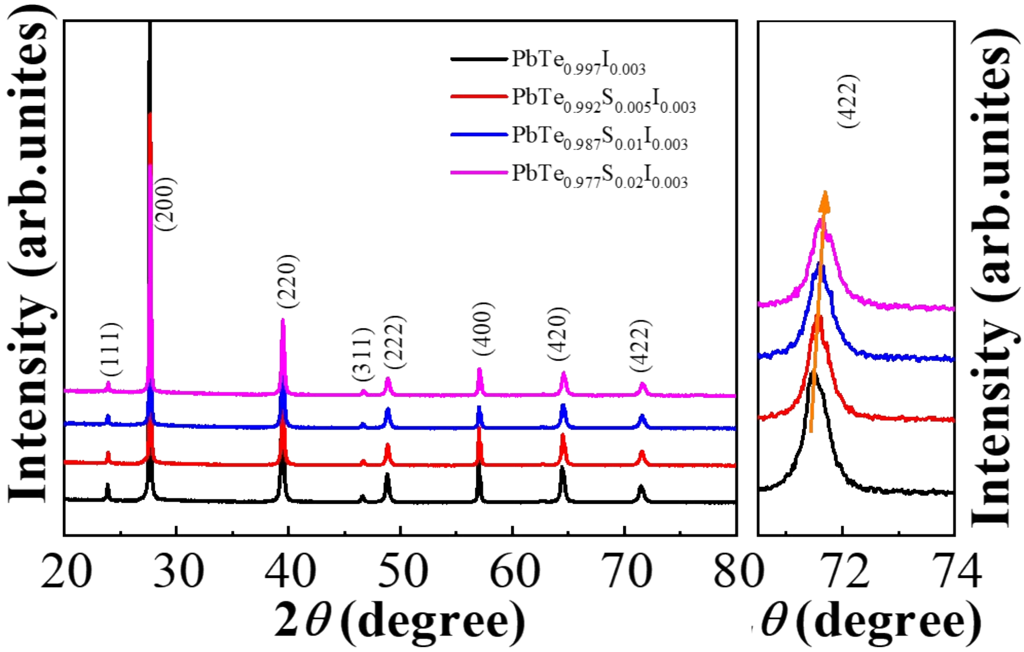

Figure S4. XRD patterns for samples of $PbTe_{0.997-y}I_{0.003}S_y$ (y =0 ~ 0.02).

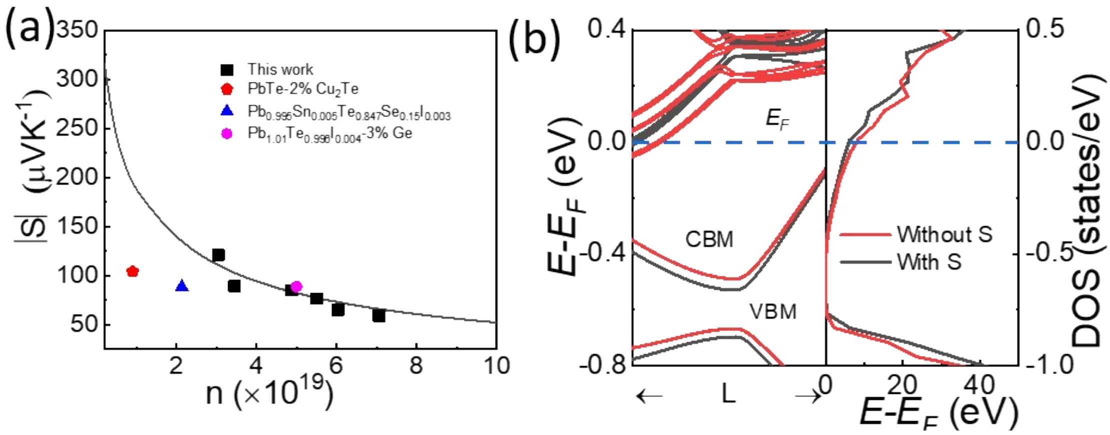

Figure S5. (a) Room temperature carrier concentration dependent Hall carrier concentration of n-type PbTe in this work compared to those reported in the literature [1-3], (b) The band structure and the density of states of S doped n-type PbTe.

Table S1. The power factor, lattice thermal conductivity, *ZT* value, of n-type PbTe-based materials with different dopants

	Max *PF* ($\mu Wm^{-1} K^{-2}$)	Min κ_l ($Wm^{-1}K^{-1}$)	Max *ZT* *T*(K)
$PbTe_{0.987}S_{0.01}I_{0.003}$ (This work)	28.7	0.47	1.73, 800
$Pb_{0.995}Sn_{0.005}Te_{0.847}Se_{0.15}I_{0.003}$ [39]	26	0.55	1.2, 673
PbTe: Gd-4%Cu_2Te [34]		~0.4	1.7, 773
PST81-0.6Sb-2Cu_2Te [53]	17.5	~0.45	1.6, 823
$(PbTe)_{0.93}(SnSe)_{0.07}$ [21]	23	0.45	1.4, 800
$Pb_{0.98}Ga_{0.02}Te$ [31]	35	0.78	1.34, 773
$PbTe_{0.998}I_{0.002}$-3%Sb [32]	31	0.6	1.8, 773
PbTe-2%Cu_2Te [38]	32	~0.5	1.5, 723
PbTe-4%InSb [33]	22	~0.3	1.83, 773
$Pb_{1.01}$Te-0.4%I-3%Ge [40]	27	0.78	1.31, 723

Table S2. The conversion efficiency of devices made of different materials

basic material	*η* (%), *ΔT* (K)	
	Single module	Segmented module
PbTe, this work	9.3, 560	12.2, 510
PbTe [54]	8.9, 570	11.02, 570
PbSe [13]	/	12.3, 510
PbS [50]	8.07, 560	11.05, 583
Half-Heusler [55]	/	12.41, 698
skutterudite [57]	/	12.0, 541
PbTe [S1]	8.5, 590	12, 590
PbTe-TAGS [S2]	6, 410	/
skutterudite [S3]	8.4, 577	/
skutterudite [S4]	8.0, 550	/

Half-Heusler [56]	6.2, 665	/

4. Intensity profile of the line and HAADF images of PbTe and $PbTe_{0.98}S_{0.02}$ after grinding in liquid nitrogen

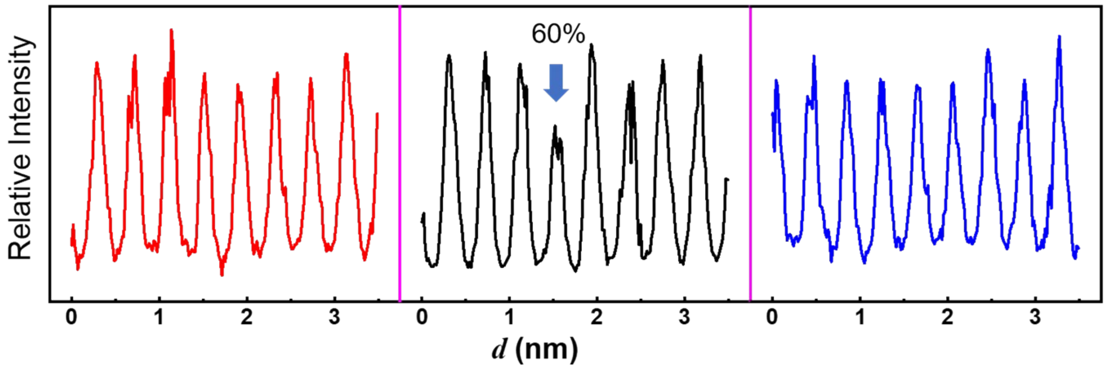

Figure S6. Intensity profile of the line shown in Fig 3 (a).

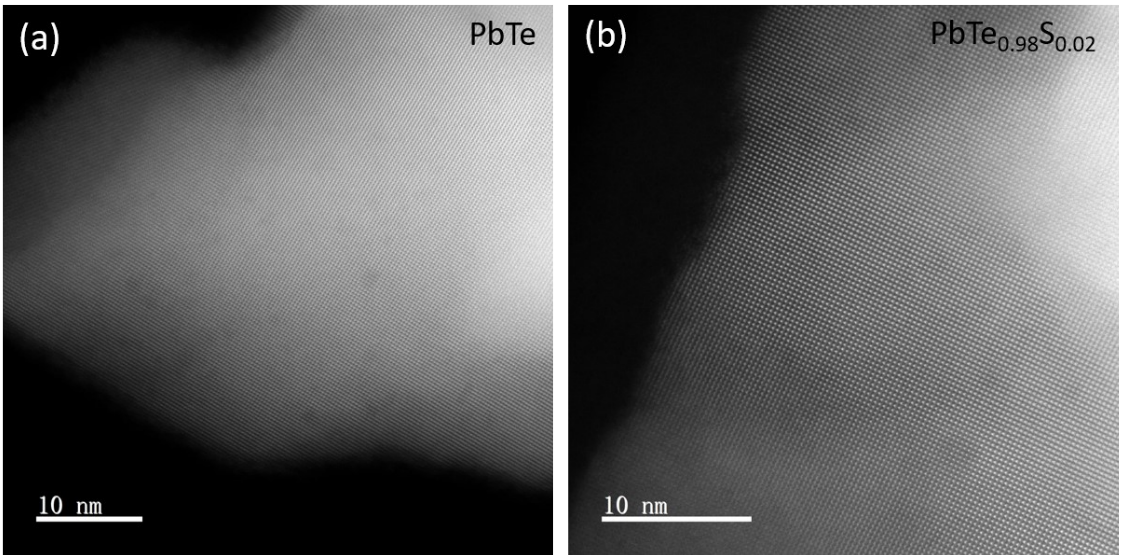

Figure S7. HAADF images of PbTe and $PbTe_{0.98}S_{0.02}$ after grinding in liquid nitrogen

Table S3. The actual composition of PbTe and $PbTe_{0.98}S_{0.02}$ characterized by EPMA, the data are obtained from different parts of the same sample.

	Elements	# 1	# 2	# 3	# 4	# 5	# 6	Average
PbTe	Pb	49.141	49.938	49.633	49.327	49.403	49.129	49.4285
	Te	50.859	50.062	50.367	50.673	50.597	50.871	50.5715
$PbTe_{0.98}S_{0.02}$	Pb	49.973	49.784	49.894	49.731	50.035	49.646	49.8438
	Te	49.297	49.767	49.434	49.692	49.344	49.824	49.5596
	S	0.73	0.449	0.672	0.577	0.622	0.53	0.5965

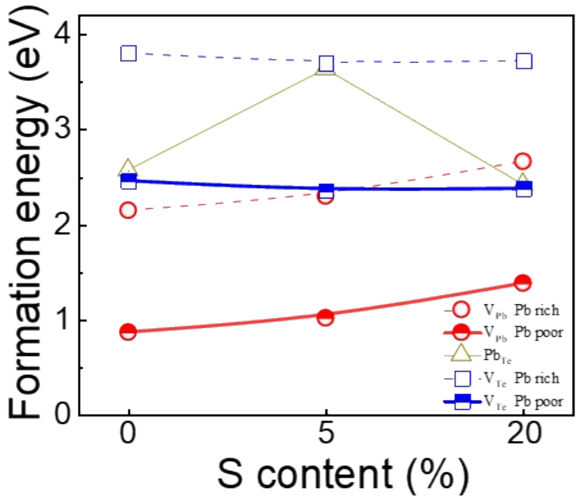

Figure S8. The formation energy of Pb vacancy (V_{Pb}), Te vacancy (V_{Te}) and antisite (Pb_{Te}) under different S content in Pb-rich and Te-rich PbTe.

5. The XRD and thermoelectric properties of $PbTe_{1-y}S_y$

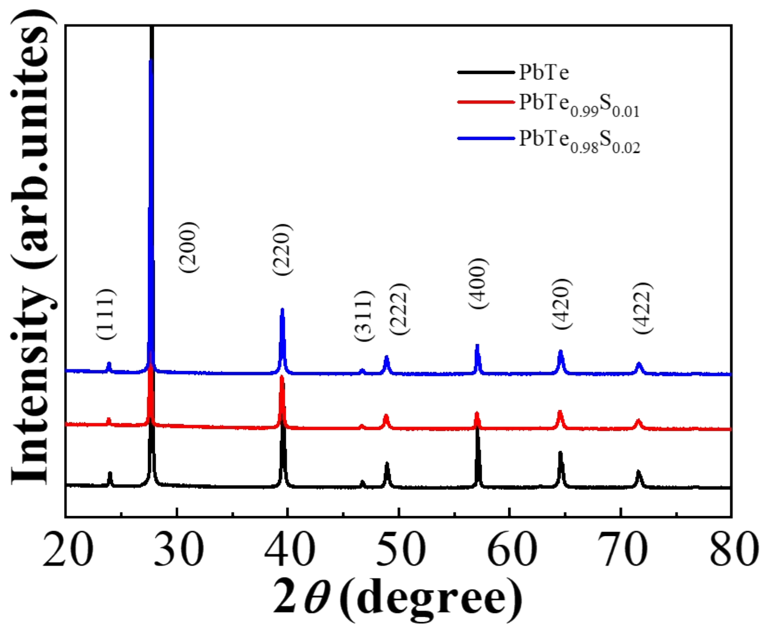

Figure S9. XRD patterns for samples of $PbTe_{1-y}S_y$ (y =0 ~ 0.02).

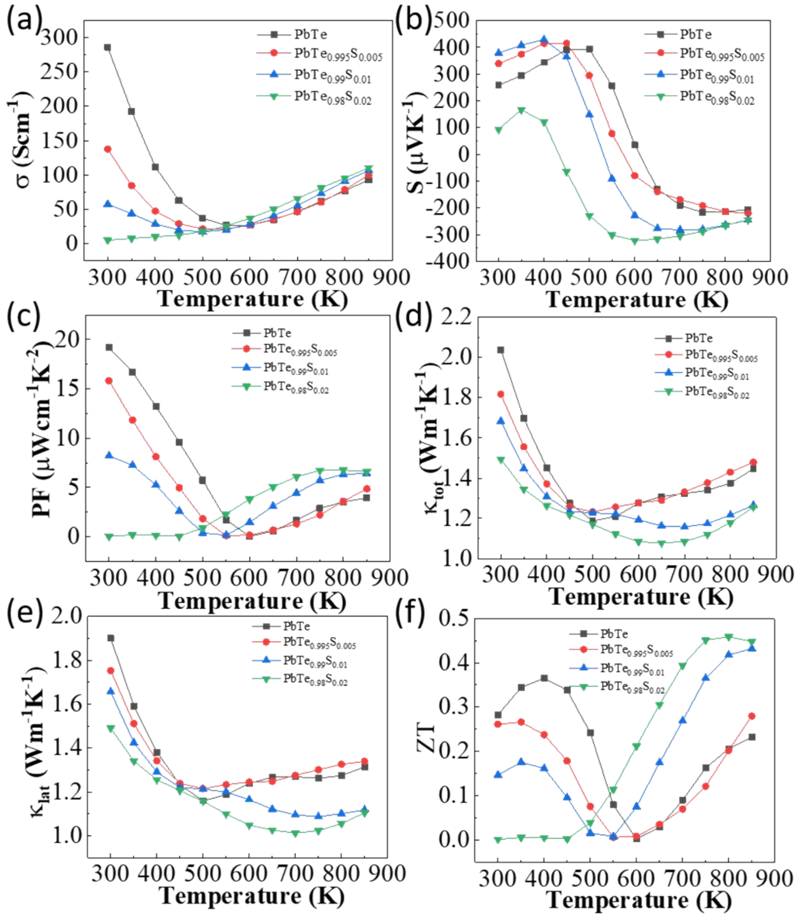

Figure S10. Temperature-dependent thermoelectric properties of $PbTe_{1-y}S_y$ (y =0 ~ 0.02), (a) electrical conductivity, (b) Seeebeck coefficient, (c) power factor, (d) total thermal conductivity, (e) lattice thermal conductivity, (f) zT value.

6. The XRD, low magnified TEM image of the $PbTe_{0.997}I_{0.003}$–2%Pb and thermoelectric properties of $PbTe_{0.997}I_{0.03}$-z%Pb

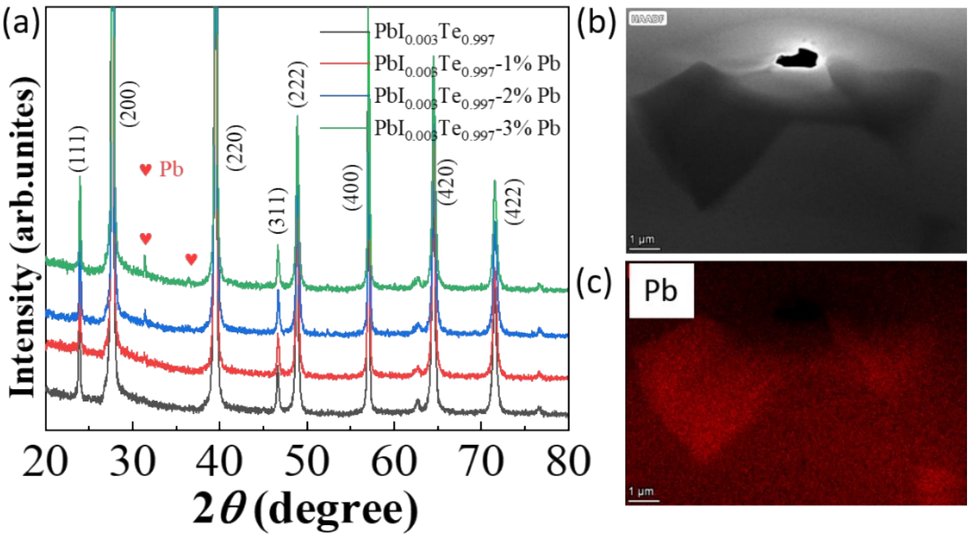

Figure S11. (a) XRD patterns for samples of $PbTe_{0.997}S_{0.003}$-z%Pb (z =0 ~ 0.03), (b) and (c) The low magnified TEM image of the $PbTe_{0.997}I_{0.003}$–2%Sb sample and element mapping, which shows that there is Pb precipitation with a size of 5mm in the material.

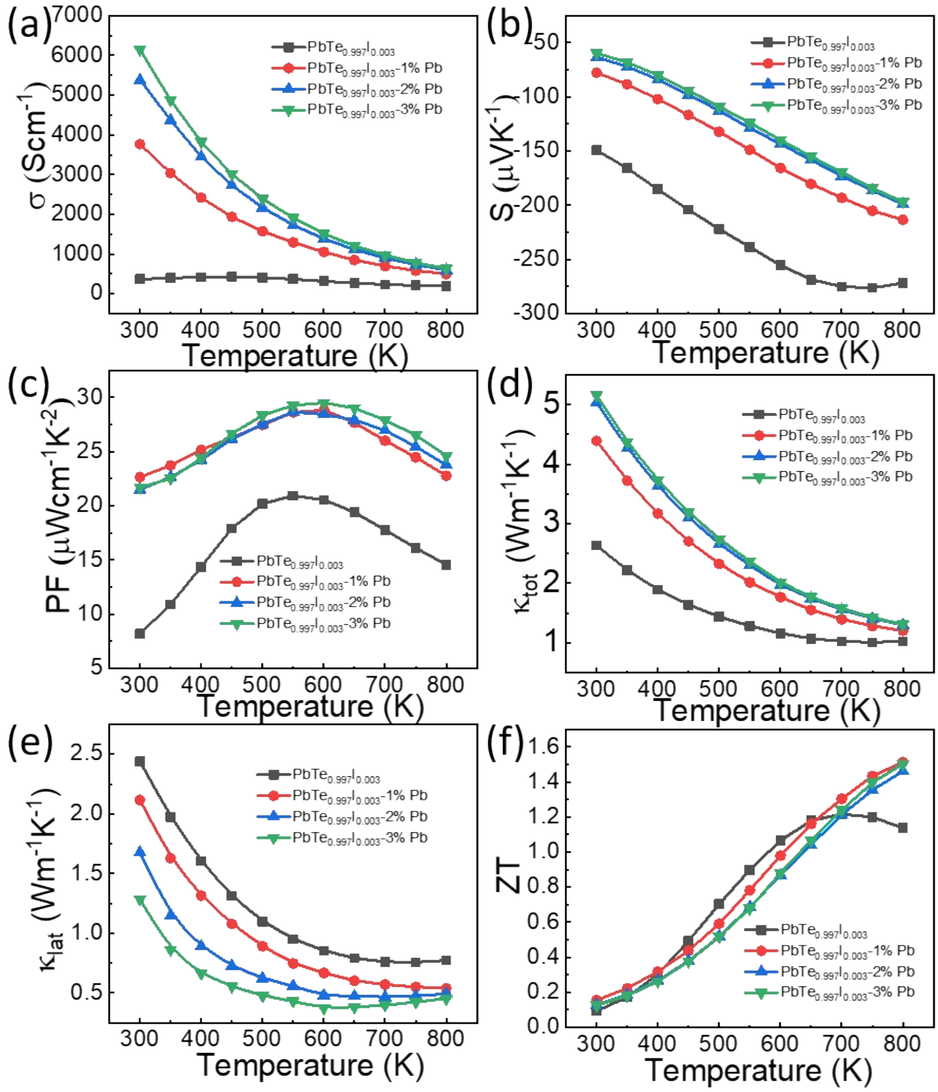

Figure S12. Temperature-dependent thermoelectric properties of $PbTe_{0.997}I_{0.003}$-z%Pb (z=0 ~ 0.03), (a) electrical conductivity, (b) Seeebeck coefficient, (c) power factor, (d) total thermal conductivity, (e) lattice thermal conductivity, (f) zT value.

Table S4 The carrier concentrations, electrical conductivities, Seebeck coefficients, carrier mobilitys, total thermal conductivities, lattice thermal conductivities and zT values of $PbTe_{0.987}S_{0.01}I_{0.003}$ and $PbTe_{0.997}I_{0.003}$-1%Pb.

Sample	$n_e \times 10^{19}$ (cm^{-3})	σ (Scm^{-1})	S ($\mu V\ K^{-1}$)	μ ($cm^2V^{-1}s^{-1}$)	$\kappa_{tot}/\kappa_{lat}$ ($Wm^{-1}K^{-1}$)	zT
$PbTe_{0.987}S_{0.01}I_{0.003}$	4.88	3399	-82.10	435	1.05/0.498	1.73
$PbTe_{0.997}I_{0.003}$-1%Pb	5.49	3767	-77.55	428	1.20/0.53	1.51

7. The complete results of single and segmented module

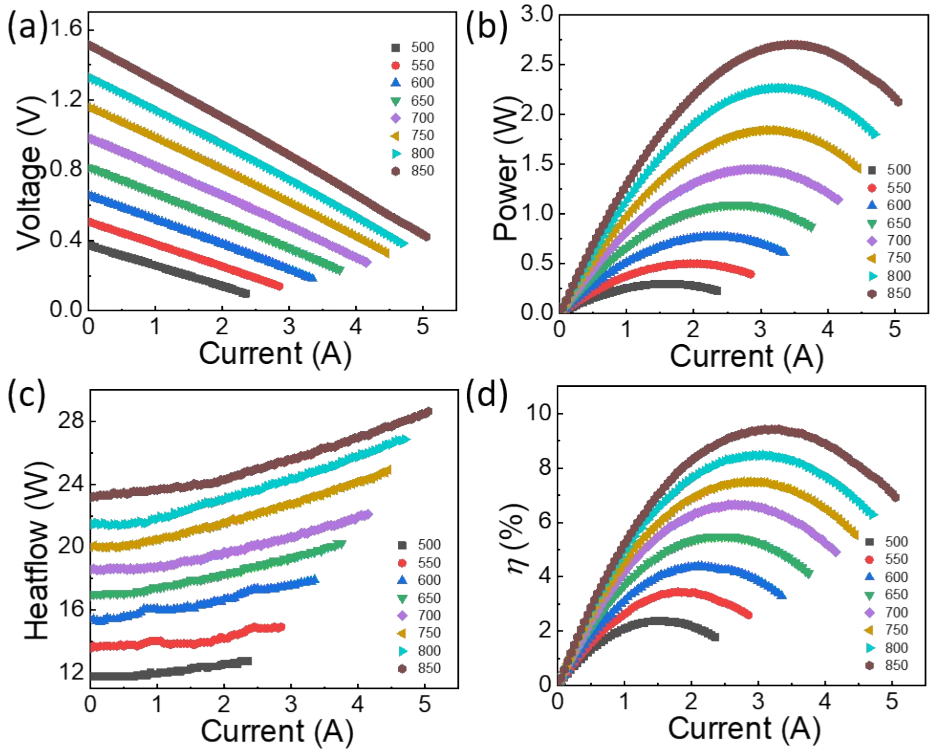

Figure S13. The measurements of single-stage thermoelectric module, (a) voltage, (b) output power, (c) heat flow, and (d) conversion efficient.

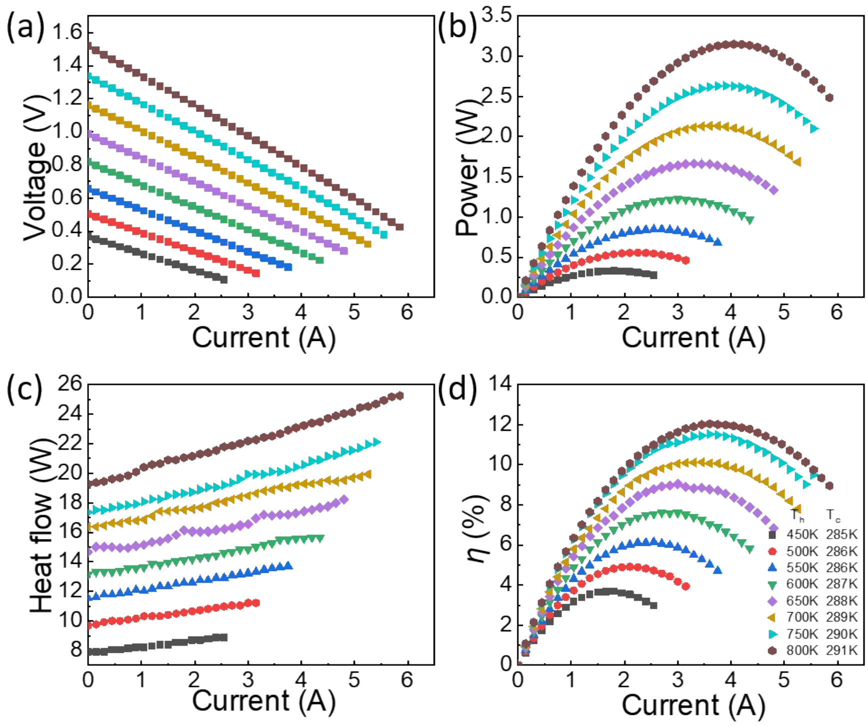

Figure S14. The measurements of segmented thermoelectric module, (a) voltage, (b) output power, (c) heat flow, and (d) conversion efficient.

References

[S1] P. Jood, M. Ohta, A. Yamamoto and M. G. Kanatzidis, Joule, 2018, 2, 1339–1355.

[S2] A. Singh, S. Bhattacharya, C. Thinaharan, D. K. Aswal, S. K. Gupta, J. V. Yakhmi and K. Bhanumurthy, J. Phys. D: Appl. Phys., 2009, 42, 015502.

[S3] P. Zong, R. Hanus, M. Dylla, Y. S. Tang, J. C. Liao, Q. H. Zhang, G. J. Snyder and L. D. Chen, Energy Environ. Sci., 2017, 10, 183–191.

[S4] J. Q. Guo, T. Ochi, S. Suzuki, M. Kikuchi, Y. Yamaguchi and S. Ito, J. Electron. Mater., 2012, 41, 1036–1042